ACS APPLIED BIO MATERIALS

www.acsabm.org Article

Gas Cluster Ion Beams as a Versatile Soft-Landing Tool for the Controlled Construction of Thin (Bio)Films

Vincent Delmez,[$] Benjamin Tomasetti,[$] Thomas Daphnis, Claude Poleunis, Clément Lauzin, Christine Dupont-Gillain,* and Arnaud Delcorte*

Cite This: *ACS Appl. Bio Mater.* 2022, 5, 3180−3192 Read Online

ACCESS | Metrics & More | Article Recommendations | Supporting Information

ABSTRACT: Surface biofunctionalization with proteins is the key to many biomedical applications. In this study, a solvent-free method for the controlled construction of protein thin films is reported. Using large argon gas cluster ion beams, proteins are sputtered from a target (a pool of pure proteins), and collected on a chosen substrate, being nearly any solid material. Time-of-flight secondary ion mass spectrometry (ToF-SIMS) revealed the presence of intact protein molecules on the collectors. Furthermore, lowering the energy per atom in the cluster projectiles down to 1 eV/atom allowed more than 60% of bradykinin molecules to be transferred intact. This protein deposition method offers a precise control of the film thickness as the transferred protein quantity is proportional to the argon clusters ion dose reached for the transfer. This major feature enables building protein films from (sub)mono- to multilayers, without upper limitation of the thickness. A procedure was developed to measure the film thickness in situ the ToF-SIMS instrument. The versatility and potential of this soft-landing alternative for further applications is demonstrated on the one hand by building a protein thin film at the surface of paper, a substrate hardly compatible with solution-based adsorption methods. On the other hand, the possibility to achieve alternated multilayer buildup is demonstrated with the construction of a bilayer composed of bradykinin and Irganox, with the two layers well separated. These results lay the first stone toward original and complex multilayers that could previously not be considered with solution-based adsorption methods, and this regardless of the substrate nature.

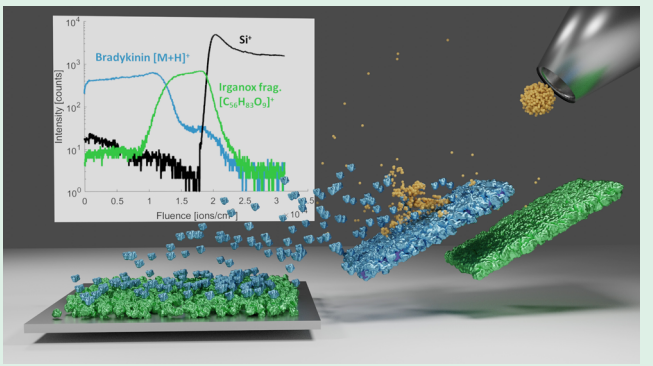

KEYWORDS: *gas cluster ion beam (GCIB), (bio)functionalization, proteins, thin films, ToF-SIMS, solvent-free deposition, multilayers*

INTRODUCTION

In the past decades, the study of surfaces has gained an enormous interest, and it has dramatically evolved, from basic surface characterization and most simple modifications, to characterization techniques that are at the cutting edge of technology, and to fabrication of nanostructured functional materials.[1−4] A multitude of surface modification techniques have been applied to inert materials to provide them with specific physical and chemical properties, leading to groundbreaking advances in many scientific fields.[5−8] More specifically, surface biofunctionalization has become a cornerstone technology for a wide range of applications including cosmetics,[9] food packaging,[10−12] biocatalysis,[13−15] and biomedical devices.[16−19] For the preparation of biomaterials, proteins, due to their myriad of different functionalities, are molecules of choice to be immobilized on surfaces. There are several well-established methodologies for the construction of protein thin films at interfaces, mostly relying on spontaneous adsorption,[20−22] or on the so-called layer-by-layer assembly method (LBL).[23] Most recent developments toward controlled protein immobilization involve more complex procedures, targeting covalent bonding to the substrate via prior protein modifications,[24−30] even though a few other original strategies were reported, such as that relying on the adsorption of protein supramolecular assemblies at interfaces.[31−33] These methods, achieved in an aqueous solution, have the advantage for some of them to be straightforward (spontaneous adsorption and LBL) and reliable for a large variety of proteins. However, they may suffer from some limitations and disadvantages. Of main concern, protein activity may be altered upon immobilization and dewetting because of conformational changes or due to reactive groups added to the protein to promote specific binding.[34,35] In addition, the deposited quantity is not always easily controlled and is usually restricted to one monolayer maximum.[36] Furthermore, there is a lack of spatial distribution

Received: February 23, 2022
Accepted: June 28, 2022
Published: July 8, 2022

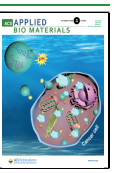

https://doi.org/10.1021/acsabm.2c00169
ACS Appl. Bio Mater. 2022, 5, 3180−3192

control, which mainly relies on patterning approaches.[37−39] Therefore, the development of alternative biofunctionalization methods offering a fine control over the resulting biofilm in terms of total protein amount, thickness, activity, patterning, mono- or multilayers composition and organization, and protein−surface interaction is highly desired.

Meanwhile, ion soft-landing, a sub-category of preparative mass spectrometry defined as the deposition of intact mass selected ions onto surfaces, has been developed as a promising and versatile tool for the solvent-free immobilization of non-volatile organic and inorganic materials.[40−42] This technique (thoroughly reviewed),[43−47] usually performed under vacuum, has demonstrated its capability to soft-land proteins with retention of their activity, using electrospray ionization (ESI) as an ion source.[48−51] Soft-landing also surpasses other deposition methods as it enables a precise control of the size, shape, position, and kinetic energy of the beam at the surface. Yet, a few obstacles still prevent soft-landing to reach commercial coating applications. These include low protein ionization yield and ion transmission, ultimately leading to very low absolute ion current and thus deposition rate.[46] Moreover, at high fluences, like-charge accumulation at the surface, may induce undesired phenomena such as repulsion effect, unfolding of proteins and uncontrolled self-organization of the layers.[45]

In the meantime, another powerful and versatile tool for processing surfaces of materials has emerged, namely gas cluster ion beams (GCIB).[52] Bombardment of surfaces by GCIB offers unique features beneficial for various industrial applications such as surface smoothing, shallow implantation, low-damage surface modification, or thin film deposition.[53−56] It also participated to the expansion of a widely used surface analysis method, time-of-flight secondary ion mass spectrometry (ToF-SIMS). The development of large argon GCIB came as a major breakthrough in the field of ToF-SIMS analysis[57,58] where it simply revolutionized the study of organic and biological materials.[59−62] Owing to their low energy per constituent atom, large argon clusters display unprecedented capabilities of eroding biomolecular films without fragmentation.[63] Recent studies have shown that proteins as large as about 12 kDa could be desorbed intact and ionized under Ar-GCIB bombardment.[64]

In 2016, Lorenz et al. showed that large argon clusters could be used to transfer organic materials from one surface onto another.[65] Later, they developed an in situ matrix-enhanced SIMS based on this transfer mechanism,[66] which was further exploited in our group.[67] Inspired by these promising results, we took advantage of the outstanding characteristics of Ar-GCIB to develop a soft-landing technique in situ a ToF-SIMS instrument. This method, consisting of bombarding a sample with an Ar-GCIB and collecting all ejected material on a desired surface, differs from other soft-landing methods mainly on two points: first, the target consists of a pure solid pool of molecules, and second, neutral molecules are transferred together with the ionized species. This latter evolution overcomes the low ionization yield inherent to existing soft-landing techniques. Previously, our group has published a proof-of-concept, as an enzyme, lysozyme, could be desorbed intact by an Ar_{5000}^{+} 10 keV cluster beam and land on a surface with retention of its activity.[68] Here, using model peptides and small proteins, we explore more in depth the impact of various experimental parameters (Ar clusters size and energy, primary ions impinging angle and collecting angle, and size of transferred biomolecule) on the efficiency of the transfer, in terms of fragmentation, deposition rate, and homogeneity of newly formed thin films. We reveal the great potential of the method to build thin films containing intact peptides and proteins, with precisely controlled thicknesses. Furthermore, we demonstrate the applicability of this deposition process for substrates that are not suitable for aqueous conditions, such as paper, and for the construction of multilayers that are difficult to obtain via other methods.

RESULTS AND DISCUSSION

Proteins Can Be Transferred Intact. To assess the feasibility to transfer intact proteins using large argon clusters, peptides were chosen as first candidates, namely, angiotensin II (human) (further referred to as angiotensin) and bradykinin, having masses of 1046 and 1060 Da, respectively. The molecular ions of these two peptides are easily detected by ToF-SIMS within regular surface analysis experiments, easing their detection on the collector after transfer. Transfer experiments were all conducted in a commercial ToF-SIMS instrument; however, the sample holder was specially designed in-house. Based on the seminal study by Lorenz et al.,[65] the target was initially placed at 30° with respect to the horizontal collector. The Ar-GCIB source was mounted at 45° with respect to a flat sample surface, and the ion beam was impinging the target with a grazing angle of 15°. This should favor a forward emission of desorbed species. Figure 1 is a schematic representation of this initial transfer geometry. Throughout this article, all impinging angles are given with respect to the target surface. Targets are always silicon (Si) wafers covered with a thick layer of molecules to be transferred. If not otherwise specified, collectors are clean Si wafers.

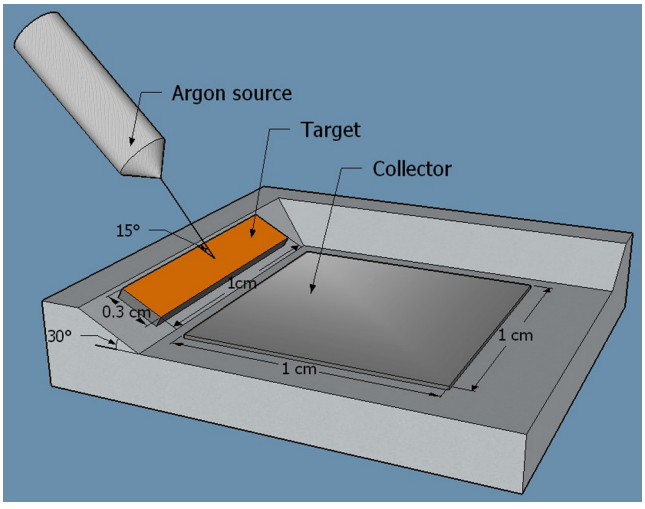

Figure 1. Schematic representation of the initial transfer geometry. The protein target is represented in orange, and the collector is represented in gray. The collector is horizontal, and the target is placed at 30° with respect to the collector. The cluster beams impinge on the target with an angle of 15°.

In this first section, transfers were achieved with an Ar_{5000}^{+} 10 keV beam. The collectors were then placed in the classical analysis sample holder and first imaged with Bi_5^{+} 30 keV using the 2D imaging mode of the instrument. It can be seen on the angiotensin collector images in Figure 2a,b that material was

https://doi.org/10.1021/acsabm.2c00169
ACS Appl. Bio Mater. 2022, 5, 3180−3192

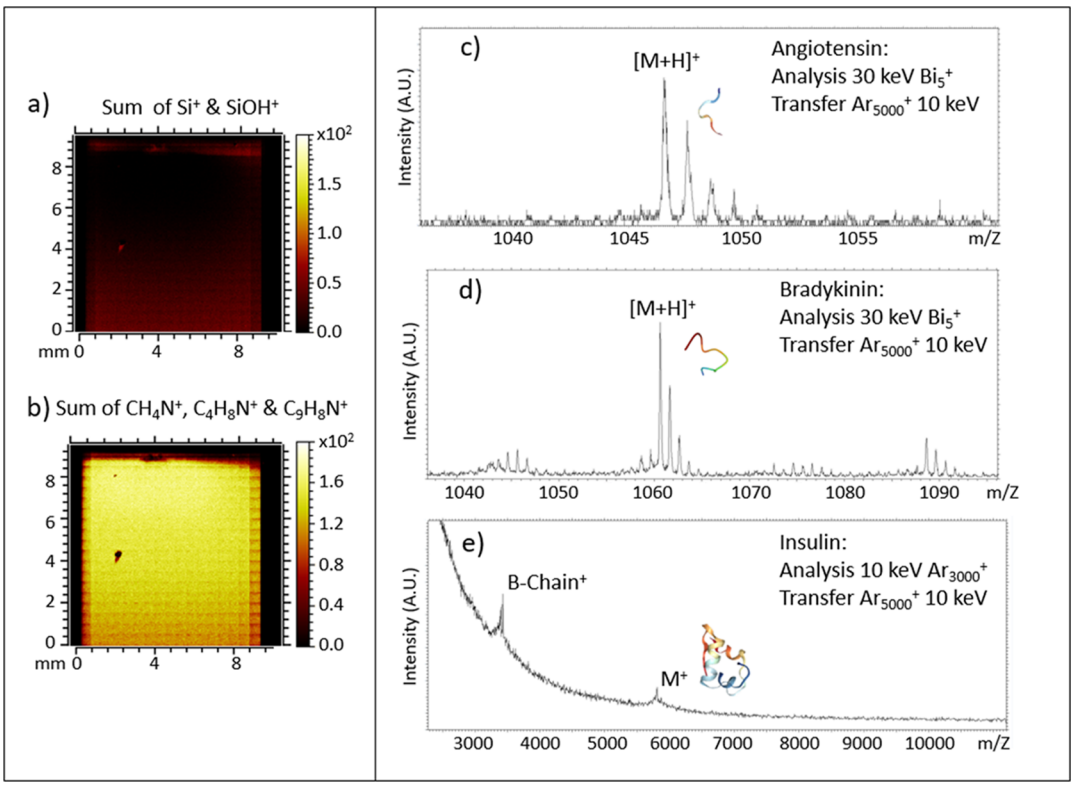

Figure 2. Left: angiotensin collector ion images. (a) Substrate intensity image, represented by the summed intensities of Si^+ and $SiOH^+$ (at m/z = 28 and 45, respectively). (b) Amino-acid material image, represented by the summed intensities of CH_4N^+, $C_4H_8N^+$, and $C_9H_8N^+$ (at m/z = 30, 70, and 130, respectively). Right: ToF-SIMS spectra recorded on collectors after transfer of (c) angiotensin, (d) bradykinin, and (e) insulin, respectively. In each case, the molecular ion is detected, demonstrating that at least a fraction of the peptides/proteins is transferred intact.

efficiently transferred from the target onto the collector. Indeed, the substrate signal intensity (Figure 2a), characterized by Si^+ and $SiOH^+$ (at m/z = 28 and 45, respectively), is attenuated on the collector, showing that an overlayer was deposited on top of it. The image of characteristic fragments of amino acids (Figure 2b), which are CH_4N^+, $C_4H_8N^+$, and $C_9H_8N^+$ (at m/z = 30, 70, and 130, respectively) confirms the protein nature of the deposited film. These specific fragments were selected as they display a high intensity in the SIMS spectra in comparison with the molecular ion. Similar results were obtained for the other transferred proteins (Figure S1). Static spectra (60 s, 30 keV Bi_5^+) were further acquired on the collectors to investigate the presence or absence of the molecular ion and thus of intact peptides. In both cases, the intact molecular ion was detected on the collector as shown in Figure 2c,d, with the usual isotopic distribution. In addition, if one compares the small mass region (<100 m/z) of the spectrum obtained on the collector with that of a reference spin-coated sample, one can observe very close resemblance in the fragmentation pattern and relative peak intensities. An exception is made for the sodium peak at m/z = 23, which sometimes displays a massive enhancement on the collector (yet never at the point where it would dominate the spectrum). In most cases, it is likely due to surface contamination of the collector prior to the protein deposition, or arises from contamination occurring between the deposition and the analysis as the samples are exposed to air when transferred to the analysis sample holder (random distribution of the sodium on the collectors). Yet, for some proteins, the sodium seems to originate from the target (sodium distribution mirroring that of the protein material). In these cases, the contamination may have occurred during the preparation of the protein stock solution. Other effects typically encountered in SIMS such as thickness, diffusion, or matrix effects may play a role in the sodium intensity variations that were observed. An example is shown for angiotensin in the Supporting Information (SI, Figure S2). These two observations demonstrate that peptides can be deposited intact using large argon clusters under UHV conditions. The challenge was then to verify this for larger biomolecules, starting with small proteins. To progress gradually, insulin, with a mass of 5808 Da was the next protein to be transferred. At the ToF-SIMS scale, insulin is already quite a large molecule, hardly detected with monoatomic beams or small clusters such as Bi_{3-5}^+. As demonstrated previously,[61] insulin can however be detected upon bombardment by large argon clusters. In this case, insulin was transferred using the same beam as the previous one, Ar_{5000}^+ 10 keV, but the collector was analyzed with Ar_{3000}^+ 10 keV. Once again, the molecular ion, corresponding to the intact protein could be detected on the collector, as depicted in Figure 2e. As for references, the fragment corresponding to the β-chain of insulin is present. The very low intensity of the intact insulin peak in the SIMS spectrum may be due to various causes and raises several comments and questions. At first glance, one may be tempted to attribute that simply to a larger fragmentation upon transfer than that observed for smaller proteins. If this is very likely to have an impact, it is certainly not the only effect to take into account. First, it should be kept in mind that even on thick reference samples, insulin is quite poorly detected in ToF-SIMS due to its mass. Second, it is expected that larger molecules are transferred with less efficiency than smaller ones (this will be discussed later),

https://doi.org/10.1021/acsabm.2c00169
ACS Appl. Bio Mater. 2022, 5, 3180−3192

and thus the amount of material available for analysis may be much smaller in the case of insulin. More experimental work would be required to precisely attribute the influence of each parameter. However, this illustrates the difficulties and limitations that are imposed by the analytical constraints of ToF-SIMS when working with larger molecules. To evaluate the transfer of larger proteins, other methods are required, as was demonstrated by our group earlier.[68] In the following sections, peptides that are easily detected in SIMS will be used as a model to study the influence of various parameters on the efficiency of transfer and to find optimized conditions that could be further used for the construction of more complex multilayers or for the transfer of larger and more complex molecules.

Primary Ion Beam Energy Effect on Fragmentation. Strictly regarding the analysis of proteins and other organic materials, argon clusters have been widely investigated and characterized. It has been demonstrated on numerous occasions that fragmentation induced during sputtering is mainly a function of the energy per atom ratio (E/n) in the clusters.[58,69] Experimental results are supported by molecular dynamic simulations.[59] It is thus expected that bombarding the target with clusters having lower E/n would prevent fragmentation and favor the transfer of intact peptides and proteins. Bradykinin (1060 Da) was transferred using Ar beams of various sizes and energies (Table 1). All Argon cluster beams distributions are shown in the SI, Figure S3. The collectors were then analyzed by ToF-SIMS using the 30 keV Bi_5^+ beam. In Figure 3, the normalized percentage of intact peptides molecules detected on the collectors is plotted in blue for each transfer condition (the reference is in green). This fragmentation is measured as the ratio "molecular ion intensity to total ion intensity" and normalized to the reference, a fresh bradykinin spin-coated sample, which is considered as 100% of intact peptides molecules. The orange closed circles represent the E/n of the clusters used for transfer. In good agreement with the literature, fragmentation of the transferred material is maximal when E/n is high (here, the highest for Ar_{1500}^+ 10 keV, 6.67 eV/atom) and then decreases with decreasing E/n, being minimal for Ar_{5000}^+ 5 keV (1 eV/atom). For the latter argon beam, it can be concluded from the comparison with the analysis of the reference that more than 60% of the collected materials are intact peptide molecules. The authors would like to emphasize on the trend of the fragmentation, clearly demonstrating that reduced fragmentation can be reached by using less energetic clusters. The values should be taken as rough estimations. Indeed, it could be biased due to different sticking coefficients of small fragments versus intact peptides or by fragmentation induced on the collector by backscattered Ar atoms, especially intense at low impinging angles such as 15° (see later). Other typical SIMS effects such as the thickness or matrix effect may influence the ionization probabilities during the analysis. In addition, an important comment must be made regarding the Ar_{5000}^+ 5 keV sample. It turns out that reducing the cluster total energy and therefore the energy per atom to such a low value significantly deteriorates the transfer efficiency at this grazing impinging angle. This observation is in line with the results obtained by Seah et al.[70] in their study of angle dependence of argon gas cluster sputtering. They showed that sputtering yields of clusters with low E/n values were much more sensitive to impinging angle variations, leading to much reduced sputtering yields at angles away from 45°. In our case, this leads to transferred quantities that are too small to be analyzed quantitatively within reasonable transfer durations. In

Table 1. Summary of the Different Cluster Beams Used to Investigate the Influence of E/n on the Fragmentation during Transfer

cluster beam	beam energy (keV)	energy per atom (eV/atom)	beam current intensity (nA)
Ar_{1500}^+	10	6.67	≈11
Ar_{3000}^+	10	3.33	≈8.5
Ar_{5000}^+	10	2.00	≈1.4
Ar_{3000}^+	5	1.67	≈1.4
Ar_{7000}^+	10	1.43	≈0.3
Ar_{5000}^+	5	1.00	≈0.2

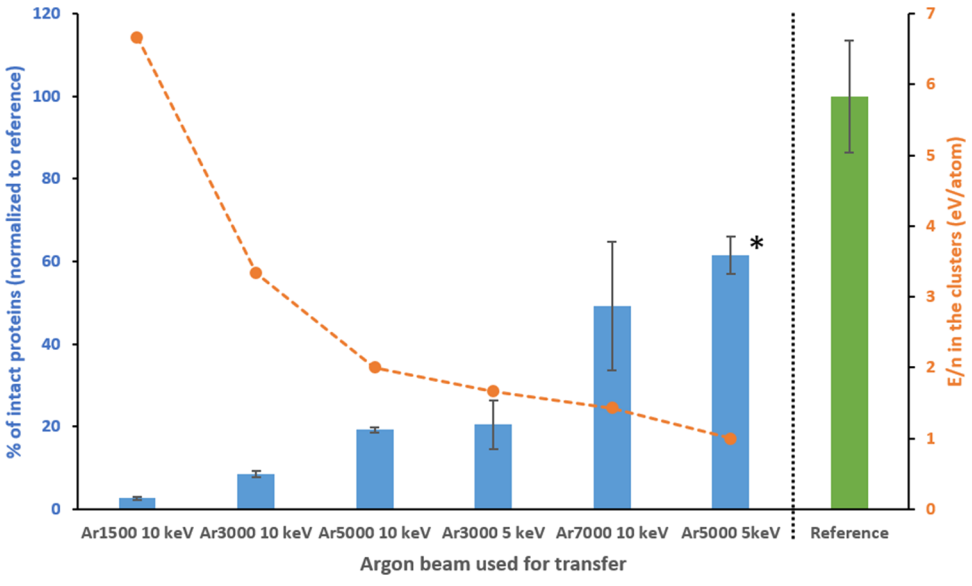

Figure 3. Fragmentation induced during transfer. For each Argon beam used for transfer, the relative percentage of intact peptides is plotted in blue. The E/n of each argon beam is plotted in orange. It is observed that the percentage of intact peptides on the collector increases as E/n decreases. *The sample Ar_{5000} 5 keV was prepared using a transfer geometry in which the target is bombarded at 45° instead of 15°.

https://doi.org/10.1021/acsabm.2c00169
ACS Appl. Bio Mater. 2022, 5, 3180−3192

fact, a minimum layer thickness is required to avoid bias in the fragmentation measurements due to the influence of the underlying hard Si substrate. As detailed by Cristaudo et al., fragmentation of organic molecules induced during analysis is favored on hard substrates for ultrathin films.[71] To tackle this issue and improve the transfer efficiency for low energy clusters, other transfer geometries in which targets are bombarded at higher angles were developed and investigated further in this study. One of these geometries showed significant improvement of the transfer efficiency and allowed a sufficient amount of proteins to be transferred using Ar_{5000}^+ 5 keV. This specific sample was therefore prepared using another geometry, which is believed to have a negligible effect on fragmentation itself. Despite these geometrical details, one must keep in mind that lowering the E/n of the clusters largely favors the deposition of intact bradykinin molecules, up to >60% in the mildest conditions investigated (Ar_{5000}^+ 5 keV, 1 eV/atom). Knowing that a large fraction of peptides/proteins molecules can be transferred intact, the next section aims at controlling the amount of proteins that is transferred and therefore the resulting film thickness.

Control of the Deposited Film Thickness and Influence of Cluster Size on Deposition Rate. As was briefly mentioned in the Introduction, controlling the quantity of deposited proteins is among the main limitations of other existing protein deposition techniques. The ones relying on spontaneous adsorption are usually restricted to the construction of a maximum of one monolayer, while the ones relying on soft landing display a very low deposition rate as only ionized species are deposited. The proposed transfer technique should allow overcoming limitations inherent to both existing methodologies. First, it is expected that the transferred amount of peptides/proteins is linearly correlated to the transfer primary ion dose. As long as the target is not depleted, there should not be a limit to the thickness that can be reached on the collector. Second, in contrast with ESI-based soft-landing, the transferred molecules are not selected in mass and therefore do not require to be ionized. All emitted species are transferred and collected, regardless of their charge state. This substantially enhances the deposition rate, enabling the construction of mono- to multilayers within a reasonable experimental time.

To ease and accelerate the thickness measurements of the deposited layer, a protocol to measure the protein thickness directly using ToF-SIMS was devised. It has been previously demonstrated in the literature that when a layer of polyelectrolytes or frozen water was deposited on top of a flat inorganic substrate, the SIMS substrate signal intensity showed an exponential decay with increasing layer thickness.[72,73] To our knowledge, this has not yet been generalized to all organic materials. Therefore, we first demonstrate that this relationship is verified in the case of peptides and proteins. For this purpose, fresh lysozyme solutions of increasing concentrations were spin-coated on silicon wafers. Their thickness was measured using ellipsometry (SI, Figure S4). These samples were then analyzed by ToF-SIMS, using the monoatomic 30 keV Bi_1^+ beam. Figure 4 shows the relative Si^+ peak intensity as a function of protein layer thickness. In good agreement with previous results, an exponential decay is observed, covering three orders of magnitude. One may notice that at both ends of this calibration, the data points are somewhat out of the exponential decay line. At very low thicknesses, this is explained by specific substrate effects on

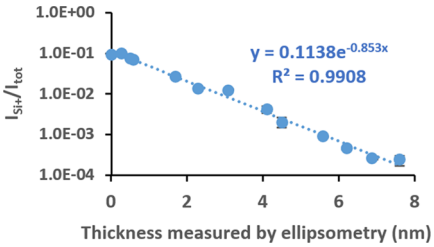

Figure 4. Exponential decay of the ToF-SIMS Si^+ substrate intensity as function of the protein layer thickness deposited on top of it. In this case, the Si^+ intensity was normalized to the spectrum total intensity to further avoid bias due to differences in the analysis conditions.

sputtering, fragmentation, and ionization, which ultimately affect the ion fractions. At thicknesses above 8 nm, the data points tend to form a plateau (not shown on the graph), mirroring the loss of the silicon signal in the noise of the spectra. Therefore, the method is not valid for thicknesses below 0.2 nm or above 7 nm. Yet, this range is sufficient to demonstrate our hypothesis that the deposited thickness is linearly correlated with the transfer ion dose and therefore can be precisely controlled.

To demonstrate this hypothesis, we proceeded as follows. For each specific cluster size, large numbers of transfers were achieved with various transfer ion doses. The collectors were then first imaged with 30 keV Bi_5^+ to ensure that deposition was efficient and that no problem occurred. Then, in the middle of the collector, successive 30 keV Bi_1^+ static spectra were acquired on a straight line, starting from the top (close to the target) to the bottom (SI, Figure S5). At each point on the collector, the Si^+ intensity of the recorded spectrum can be transformed into protein thickness, ultimately yielding a thickness profile of the collector, as can be seen in the SI, Figure S5. The initial transfer geometry leads to a non-uniform film thickness on the collector as more material is deposited close to the target. Therefore, to compare the transferred quantity on different samples, we compare the maximum thickness measured on each collector (example given for lysozyme transferred with 10 keV Ar_{3000}^+ in SI, Figure S6). Transfers were performed for bradykinin with various Ar_n^+ beams (n = 1500, 3000, and 5000) and various transfer ion doses for each beam. All collectors were studied as described above, and finally, the maximum thicknesses measured on each collector were plotted as a function of transfer ion dose, as shown in Figure 5. One can observe that for each cluster beam, the maximum thickness of the deposited films is increasing linearly with the transfer ion dose. This demonstrates that by controlling the transfer ion dose, it is possible to finely tune the thickness of the deposited films, from sub mono- to multilayers of proteins. Lysozyme and bradykinin have sizes of roughly 3.5 and 1.1 nm, respectively, so that when a 7 nm film is deposited, it corresponds to approximately 2 and 6 layers of each protein. Regarding the efficiency of the transfer between different cluster sizes at an equivalent total energy of 10 keV (and therefore different E/n), it was expected that higher E/n clusters would favor desorption and thus display a higher deposition rate. If this was verified for the transfer of bradykinin with Ar_{5000}^+ and Ar_{3000}^+, the deposition rate observed for Ar_{1500}^+ was surprisingly low. Taking a closer look at the amino acid material images of the collector, as shown for example for the molecular ion image of angiotensin transferred by 10 keV Ar_{5000}^+, Ar_{3000}^+, and Ar_{1500}^+ (Figure 6a),

https://doi.org/10.1021/acsabm.2c00169
ACS Appl. Bio Mater. 2022, 5, 3180−3192

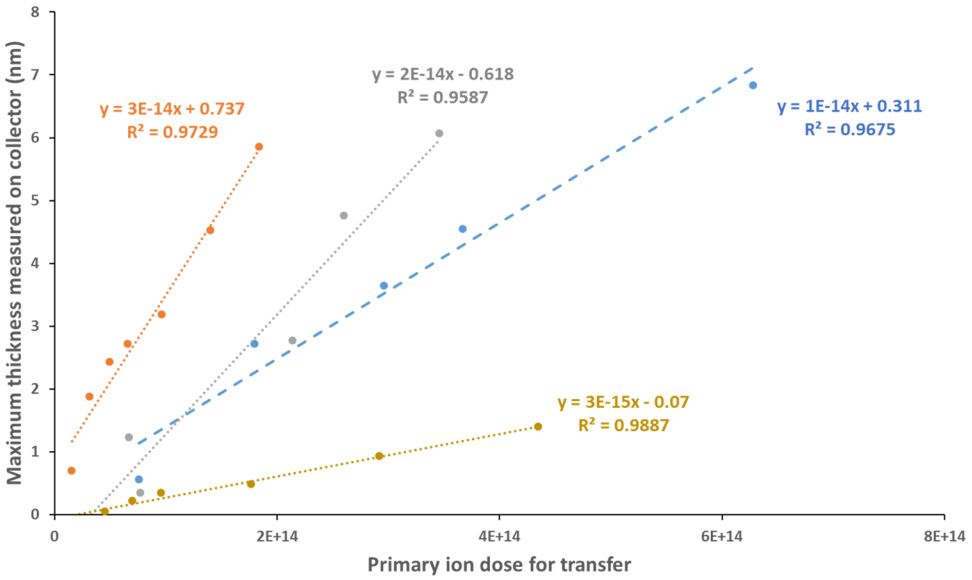

Figure 5. Linearity between the transfer ion dose and the amount of proteins deposited. The maximum thickness measured on each collector is plotted as function of the transfer ion dose. In fact, each data point represents an individual transfer. In orange, gray, and yellow, bradykinin was transferred using a 10 keV Ar_{3000}^+, Ar_{5000}^+, and Ar_{1500}^+, respectively. In blue, lysozyme was transferred using a 10 keV Ar_{3000}^+. In each case, the maximum transferred thickness could be linearly correlated to the transfer ion dose.

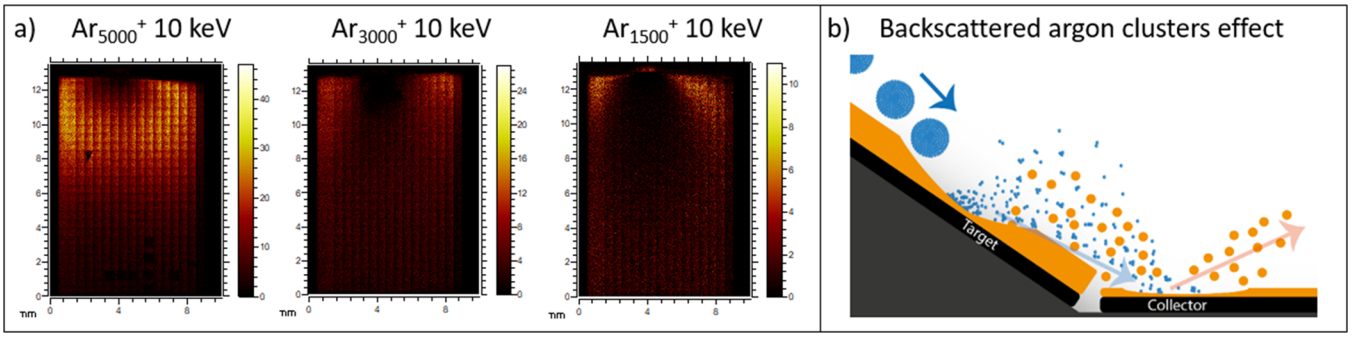

Figure 6. (a) Molecular ion images (ToF-SIMS) of angiotensin, transferred with various 10 keV Ar_n^+ beams. A shadowed area where fewer peptides were deposited is observed for each transfer condition and is gradually increasing with increasing E/n in the clusters. (b) Schematic illustration of the backscattering of argon particles (atoms and small clusters) to explain the presence of the shadowed areas shown in (a). Peptide/protein materials are represented in orange, while the argon atoms are represented in blue.

one notices that an area in the center top of the collector is shadowed, as if less material was deposited in that spot. This effect may be attributed to the backscattered argon atoms and small clusters, resulting from the dissociation of the large primary clusters upon impact with the target surface. Indeed, under this grazing angle impact, the backscattered particles tend to keep a forward direction and so are sent toward the collector, as illustrated in Figure 6b. This is supported by molecular dynamic simulations.[74] The shadowed area becomes larger from Ar_{5000}^+ to Ar_{1500}^+, mirroring the increase of the E/n of the clusters. Most likely, backscattered projectile atoms that reach the collector with sufficient energy may lead to degradation and further sputtering of the protein fragments from the collector. The final deposited amount of material and the deposition rate would then depend on the balance between the total transferred quantity and the fraction desorbed from the collector for each cluster impact. If the deposition is largely favored for Ar_{5000}^+ and Ar_{3000}^+ due to their low E/n, deposition and desorption seem to be more balanced for Ar_{1500}^+, explaining the low deposition rate observed in Figure 5.

The same procedure was applied to lysozyme, with 10 keV Ar_{3000}^+. Here, again, a linear correlation could be established between the deposited thickness and the transfer ion dose (Figure 5, blue line). As expected, the deposition rate is lower for lysozyme than for bradykinin, as lysozyme is roughly 14 times larger. This gives a first insight into a potential limitation of the technique, if much larger molecules with lower sputtering yields need to be deposited. Nevertheless, this drawback could be compensated for by optimizing the transfer geometry and consequently substantially enhance the deposition rate. This point is investigated in the following section.

Improved Transfer Geometries. As mentioned in the previous sections of this paper, the initial transfer geometry (Figure 1), that is, an incident angle of the Ar cluster beam of 15° and a collecting angle of 30° might not be optimal (see ref 56 and MD simulation).[74] Most importantly, the sputtering yield is low at such a low angle. In addition, a clear thickness gradient is observed on the collectors, mirroring the angular distribution of the ejecta. To improve both the deposition rate and the thickness uniformity, a few other transfer geometries were investigated. For each targeted geometry, a specific

https://doi.org/10.1021/acsabm.2c00169
ACS Appl. Bio Mater. 2022, 5, 3180−3192

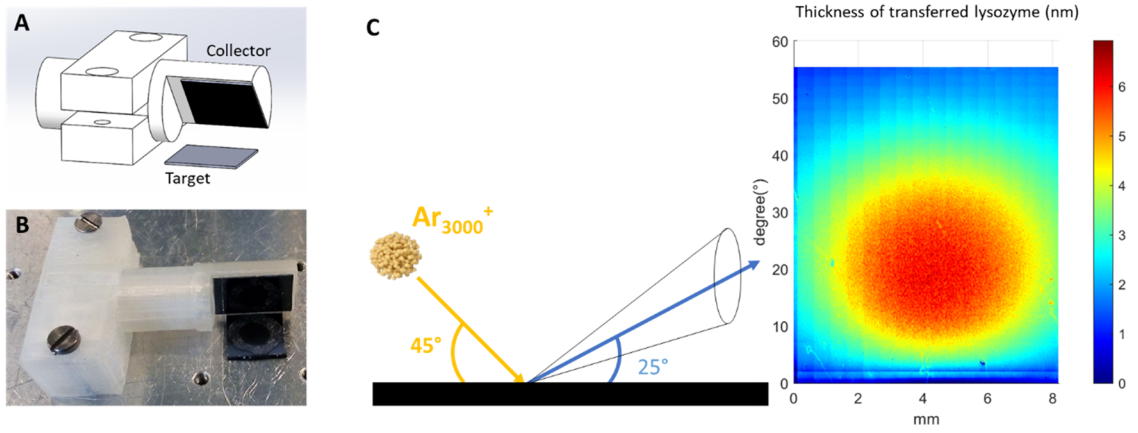

Figure 7. (a) Design of the PLA sample holder, with the horizontal target for an optimal desorption (argon clusters impact at 45°) and the collector on a rotating part that allows a wide range of collecting angles. (b) Picture of the actual printed sample holder with here the collector set at 90°. (c) Representation of the transfer geometry with an Ar beam impact angle of 45° (dark yellow) and the collector, illustrated by the thickness map of the deposition, placed at 90° from the horizontal target (black). The maximum of the distribution was observed at 25° (blue). In this case, lysozyme was transferred with 10 keV Ar_{3000}^{+}.

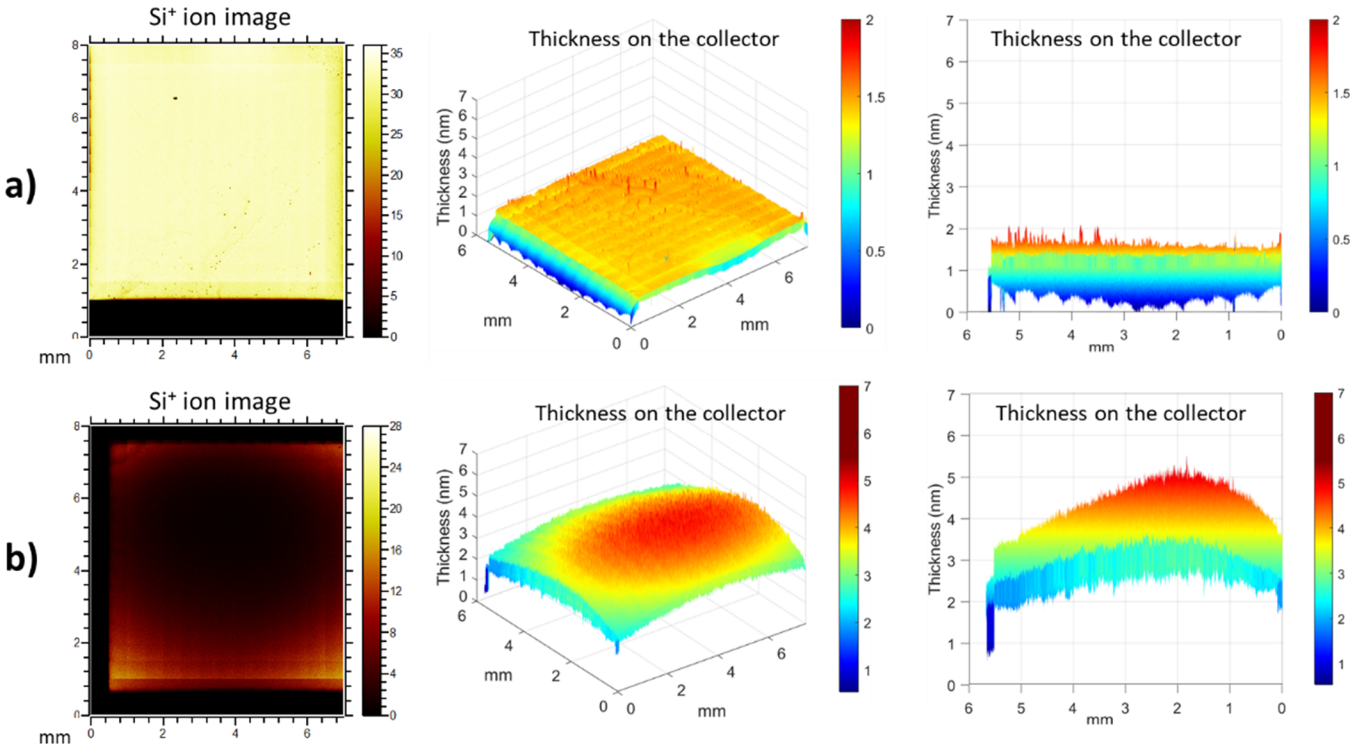

Figure 8. Comparison between Ar_{3000}^{+} transfer of lysozyme with incident angles of (a) 15 and (b) 45° for a dose of 1×10^{14} ions (15 min). ToF-SIMS chemical images of the Si^{+} substrate intensity were acquired with 30 keV Bi_1^{+}. The thickness maps were obtained using the MATLAB app (AppTBB1). Both transfers were reproduced twice without any changes in the results.

sample holder was 3D-printed in polylactic acid (PLA). Among all 3D-printed transfer sample holders, one stands out by its simplicity of use, the versatility in the angles it allows, and the results it yielded. This sample holder will be described in more details and used to gather all data shown in the following discussion. The others are presented in the SI, Table S1, with a short description and their advantages/disadvantages. In the sample holder of interest, depicted in Figure 7a,b, the target is horizontal, for an optimal Ar beam incidence angle (45°), and a rotating part allows the collection angle to be varied. In the first experiment, in order to observe the angular distribution of the proteins, the collector was placed at 90° from the target. As reported by Lorentz et al. for Irganox,[65] the sputtered proteins are ejected at average polar angles smaller than 45° with respect to the horizontal target surface. Figure 7c illustrates this for lysozyme sputtered with 10 keV Ar_{3000}^{+}, with the maximum of the deposition detected at 25°. As observed in Figure 7c, all sputtered molecules are collected, as the collector is larger than the ejection cone at the collecting distance. This implies that the collecting angle (fixed angle of the collector on the sample holder) does not have a major impact. In the following, and strictly for technical reasons (ease of focusing the Ar cluster beam impact point on the target), the collector was systematically placed at 45° from the target.

https://doi.org/10.1021/acsabm.2c00169
ACS Appl. Bio Mater. 2022, 5, 3180−3192

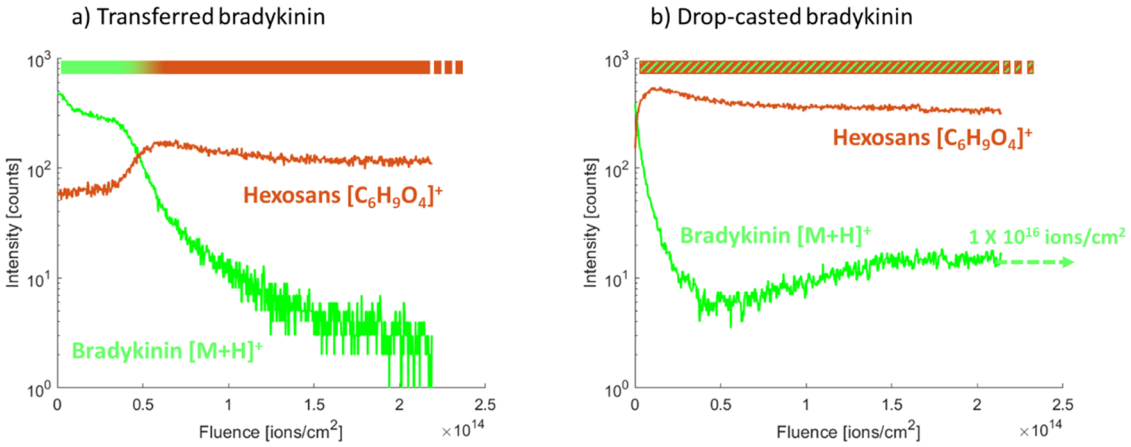

Figure 9. ToF-SIMS depth profiles recorded on the collectors after deposition of bradykinin on paper by (a) transfer or by (b) drop-casting.

Note that the deposited film thickness maps, such as those displayed in Figures 7 and 8, were obtained by imaging the entire collector with 30 keV Bi_1^+. This time-consuming analysis generates a huge quantity of data. To facilitate the data analysis and allow a rapid conversion of the Si^+ signal intensity into protein thickness, an application was developed in both PYTHON (pyTBB1) and MATLAB (AppTBB1). These platforms, Thickness By Bi1, allow to load the raw substrate intensity image, perform normalization, transform the Si^+ intensity into protein thickness using the calibration, and offer a multitude of options to display the resulting thickness maps in a user friendly way, as shown in Figures 7 and 8. These tools could easily be used for thickness measurements of other materials as parameters of the calibration can be tuned directly in the app. The app and a discussion of the methods and analyses are made available in the extensive Github platform https://github.com/Benjamin-sc/TBB1.

Figure 8 compares two 10 keV Ar_{3000}^+ transfers of lysozyme conducted with the same ion dose (1×10^{14} ions, equivalent to approximately 15 min of sputtering). For an incident angle of 15°, the amount of transferred material is extremely small. Moreover, a small crater is observed at the edge of the collector, attributed to energetic backscattered argon particles (as discussed earlier). For an incident angle of 45°, much more material is transferred and the silicon substrate is almost entirely covered. To characterize more precisely the deposition rate enhancement, a series of transfers of lysozyme was achieved with 10 keV Ar_{3000}^+, in the same fashion as in Figure 5, blue data points. Using this 45° transfer geometry, an 8-fold increase of the deposition rate was observed, as displayed in the SI, Figure S7. In addition, there is no more cratering on the collector. Indeed, at 45°, the argon clusters penetrate more deeply in the target and therefore release more of their energy during the impact.[74] The backscattered particles thus have little remaining energy and do not induce sputtering if the collector is reached. Homogeneity of the deposited films is still not perfect but is also largely improved using this geometry. It could be further improved simply by moving the *X* and *Y* positions of the Ar beam on the target during the transfer.

Toward Useful Applications: Substrate Versatility and Mixed Multilayer Construction. In the previous sections of the paper, we thoroughly investigated the technical aspects and the effect of operational parameters on this argon cluster-assisted protein deposition method. We already showed that it could overcome limitations inherent to existing protocols such as aqueous adsorption or ESI-based soft-landing by building multilayer regime thin films of precise thicknesses in relatively short times. To further demonstrate the potential of this deposition method, as well as its versatility, this section focuses on the preparation of original samples that would be otherwise very challenging to obtain using existing methods. For example, the most widespread method, spontaneous adsorption in solution, faces difficulties to build alternated multilayers, and completely fails if the targeted substrate is soluble or may be altered by the solution.

First, we illustrate the versatility of the method in terms of the substrate nature by building a peptide (bradykinin) layer on top of a sheet of paper, which is hardly compatible with solution-based methods (swelling effect). We compare the resulting sample with that obtained by drop casting a peptide aqueous solution directly on the paper substrate to mimic aqueous adsorption (not possible as paper would suffer structural deformation, making further ToF-SIMS analysis impossible). The transferred sample was prepared with a 10 keV Ar_{3000}^+ beam, while the drop-casted sample was prepared by evaporating a 10 μL drop of a 20 mg/mL solution. Both samples were analyzed by ToF-SIMS, using the 3D depth-profiling mode that allows digging in the sample by removing layers of material between sequential analyses. Figure 9 shows the comparison of the depth profiles obtained for each sample. The paper is identified in the spectra by the presence of the hexosan peak $[C_6H_9O_4]^+$, a characteristic fragment of cellulose, while bradykinin is identified by its molecular ion peak. When the peptide is transferred (Figure 9a), the paper substrate (orange signal) is covered by a layer of bradykinin (green). After a certain fluence, the bradykinin signal drops drastically until reaching the noise level. At the same time, the paper signal increases and becomes constant at a high intensity. This shows that the transfer method allowed the construction of a peptide layer strictly on top of the paper, without diffusion into the cellulose fiber network. In contrast, when the peptide is drop-casted from water (Figure 9b), the signal of bradykinin (green) instantly decreases and then levels off at a substantial intensity. It remains constant up to a sputtering dose of 1×10^{16} ions/cm^2. The paper signal (orange) remains roughly constant throughout the entire profile. If the initial drop of the bradykinin signal may suggest a partial accumulation of the peptide at the surface, the continuous detection of bradykinin across the paper indicates that the peptides diffused between the cellulose fiber of the network or directly in swollen fibers.

https://doi.org/10.1021/acsabm.2c00169
ACS Appl. Bio Mater. 2022, 5, 3180−3192

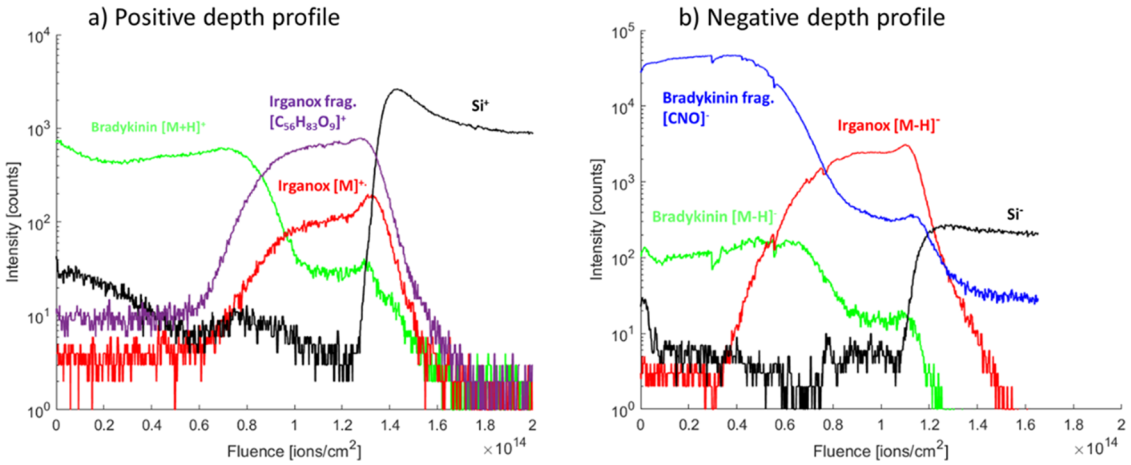

Figure 10. (a) Positive and (b) negative depth profiles of a mixed multilayer constructed by successive transfer of Irganox and bradykinin on a silicon substrate.

Chemical images acquired at the surface and inside the paper for both samples can be found in the SI, Figure S8. In addition, the deposition of a drop on the paper causes mechanical deformation of the paper and generates huge roughness. The transfer method allows the deposition of peptides/protein thin films on substrates that could not be considered when working in an aqueous solution. This demonstration using paper paves the way to many other original systems that could previously not be envisaged, such as deposition on a sacrificial layer, for further release applications, or simply on soluble substrates.

Second, we investigate the construction of mixed multilayers, composed of various species. In the present case, bradykinin and Irganox 1010 ($C_{73}H_{108}O_{12}$, Mw = 1176.7 g/mol) were chosen, as both molecular ions are detectable in ToF-SIMS without interfering with one another. A 10 keV Ar_{3000}^{+} beam was used to transfer both compounds, each time reaching an ion dose of 5×10^{14} ions. In the first place, bradykinin was deposited on top of Irganox. The two transfers resulted in a total thickness of approximately 150 nm (measured by profilometry), which makes the deposited film visible to the naked eye (SI, Figure S9). The sample was then depth-profiled by ToF-SIMS, in both positive and negative polarities. The profiles are shown in Figure 10. As the bradykinin molecular ion peak is not very intense in the spectra in negative polarity, a characteristic fragment was added. The same was applied for Irganox in positive polarity. The profiles show that the multilayer was nicely constructed, as the two layers are discernable. Yet, one may notice that the bradykinin signal does not immediately drop to minimal intensity when Irganox starts to be detected. A plateau of low intensity is maintained through the Irganox layer. If the cause of this observation is not yet undisputedly attributed, it may be explained by inhomogeneity of the layers across the probed area or by mixing, happening when bradykinin molecules are landing on the Irganox layer. The same depth profiles were performed after exposure of the sample to atmospheric conditions for 7 days (SI, Figure S10). Those profiles look the same as the ones performed on the fresh sample, confirming the stability of the multilayer construction. The reverse multilayer, with Irganox on top of bradykinin, was also constructed. Once again, the profiles, shown in the SI, Figure S11, confirmed that the two distinct layers could be obtained. For this construction, a plateau of low intensity of Irganox is visible through the bradykinin layer. This would favor the hypothesis that the species transferred in a second stage impinge the collector with sufficient energy to penetrate in the former layer and generate molecular mixing. Further experimental work such as transfer with a lower E/n argon beam would be needed to confirm this hypothesis and improve layer separation. However, the mixing remains almost negligible, as the intensity of the observed plateaus is very low.

CONCLUSIONS

A versatile solvent-free method for the construction of peptide/protein thin films was successfully developed. It expands the scope of existing approaches with a straightforward control of the deposited thickness up to multilayers and with its ability to build protein films on virtually any vacuum-compatible solid substrate. In this method, large Ar-GCIBs are used in vacuo to sputter proteins from a target onto a collector. Three model peptides and proteins, which are angiotensin, bradykinin and insulin, could be deposited intact as their molecular ions were detected on the collectors by ToF-SIMS. Soft transfer conditions were achieved by reducing the cluster E/n to 1 eV, enabling bradykinin to be transferred with as much as 60% of intact molecules. The exponential decay of the SIMS substrate intensity with the growing thickness of the protein overlayer enabled the establishment of a procedure to measure the deposited film thickness directly using the ToF-SIMS instrument. It was further demonstrated that as long as the target is not depleted, the transferred quantity is linearly correlated to the Ar cluster transfer ion dose, offering a precise control over the deposited film thickness, without upper limitation. Finally, the potential of this cluster-assisted deposition method was exemplified in two ways. First, flexibility toward the substrate nature was demonstrated by deposition of a protein thin film on the surface of paper, a material hardly compatible with the solution-based adsorption method. Second, the possibility to build more complex architectures was validated by the construction of a bilayer composed of bradykinin and Irganox. This work provides an alternative protein deposition method that will further lead to preparation of original and complex sample architectures that could not be considered previously.

https://doi.org/10.1021/acsabm.2c00169
ACS Appl. Bio Mater. 2022, 5, 3180−3192

MATERIAL AND METHODS

Targets and Collectors Preparation. Depending on the setup geometry, the targets were thick (0.73 mm) 1 × 0.3 cm^2 rectangular or 1 × 1 cm^2 square silicon (Si) wafers (for the 15 and 45° impinging angle geometries, respectively). Prior to protein deposition, wafers were cleaned for 15 min in a piranha mixture (sulfuric acid/hydrogen peroxide, 4:1) and then underwent a UV-ozone treatment for 15 min. Angiotensin II (human), bradykinin, insulin, and lysozyme were purchased from Sigma-Aldrich (Steinheim, Germany) and used without further purification. For each peptide/protein, a concentrated aqueous stock solution at 20 g/L was prepared and stored at −20 °C. Targets were prepared by three consecutive depositions of a 10 or 20 μL drop of this stock solution for the small and large targets, respectively, resulting in a thick dry protein layer of about 23 and 15 μm in thickness, respectively. Thickness data were obtained by measuring the depth of the crater by profilometry (Bruker Dektak XT 0.7 μm, Bruker UK Ltd) after sputtering the target until the Si substrate was reached. The targets were uniform in terms of thickness, yet the surface roughness of these dried-drop thick layers was relatively important. The topography was measured with the profilometer prior to the transfer experiment and revealed a peak-to-valley value of about 200 nm. Targets were kept at room temperature for no longer than 7 days before use.

If not otherwise specified, collectors were thin (0.31 mm) 1× 1 cm^2 square Si wafers. Collectors were cleaned just before being inserted in the SIMS, following the same cleaning procedure as for target substrates.

Spin-Coated Samples. All protein reference SIMS spectra were obtained on spin-coated samples of fresh protein, prepared with a spin-coating instrument (WS-400B-6NPP/LITE, Laurell, USA). After cleaning, a drop of 150 μL of a solution of fresh angiotensin, bradykinin, insulin, or lysozyme (1 g/L) was deposited on the collector, which was then spun at 3000 rpm for 1 min (acceleration 1064 rpm/s).

Ellipsometry Measurements. Thickness measurements achieved by ellipsometry were done using an Accurion EP3+ SW (Accurion GmbH, Göttingen), with a refractive index (n) and an extinction coefficient (k) fixed at 1.5 and 0, respectively, for the fitting process of all proteins.

Molecular Transfer and ToF-SIMS Analysis. A TOF.SIMS 5 (ION-TOF GmbH, Münster, Germany) time-of-flight secondary ion mass spectrometer was used both for transfer experiments and for analysis of the collectors. The instrument is equipped with a bismuth liquid metal ion gun (LMIG) and an argon gas cluster ion beam (Ar-GCIB), both mounted at 45° with respect to the horizontal sample surface. The time-of-flight mass analyzer is perpendicular to the sample surface. Secondary ions are accelerated at a potential of 2 kV.

For the transfer experiments, the sample holder with target and collector plates was aligned with the GCIB (Figure 1). The alignment was done by sight for the x and y coordinates and using the laser that is coaxial with the analyzer for the height z. The Ar-GCIB source was operated at 5 or 10 keV, and the cluster distribution was selectively centered on Ar_{1500}^+, Ar_{3000}^+, Ar_{5000}^+, or Ar_{7000}^+. The Ar-GCIB was used in interlaced sputter mode, with the analysis beam shut down during the entire transfer. The current intensity was measured each time prior to experiment and was slightly fluctuating around 12, 8, 1.4, and 0.3 nA for 10 keV Ar_{1500}^+, Ar_{3000}^+, Ar_{5000}^+, or Ar_{7000}^+ and around 1.4 and 0.2 nA for 5 keV Ar_{3000}^+ and Ar_{5000}^+, respectively. The beam raster was fixed at 128 × 128 data points over an area of 700 × 700 μm^2. The total ion dose reached for the transfers was in the range of 10^{13}–10^{15} ions.

The analyses of the collectors were performed in a regular sample holder, using static mode (defined by an ion dose $\leq 10^{13}$ ions/cm^2) and 2D imaging modes of the instrument. In this latter operating mode, the beam moves automatically along the sample surface and gathers multiple square images to build the total image of the collector. The beam was either Bi_1^+ or Bi_5^+ 30 keV having a current intensity of about 1.4 and 0.1 pA, respectively, with a raster of 128 × 128 data points over an area of 500 × 500 μm^2. Static spectra were acquired for 60 s. For the images, a single scan was performed, but 2 and 37 frames, for Bi_5^+ and Bi_1^+, respectively, were taken on every 500 × 500 μm^2 patch to increase signal intensity. Except if otherwise specified, only positive secondary ion species were analyzed. With Bi_5^+ 30 keV, a resolving power of $m/\Delta m \approx 4300$ at 30 m/z (corresponding to CH_4N^+) was maintained for spectra acquisition. In the case of Bi_1^+ 30 keV, the resolving power was maintained around 6000 at 30 m/z.

SIMS depth profiles were recorded both in positive and negative ion polarities. The dual beam mode was used (illustrated in the SI, Figure S10d). A 10 keV Ar_{3000}^+ beam was employed to sputter material with a raster fixed at either 600 × 600 or 1000 × 1000 μm^2. Depending on the sample thickness, the sputter beam current was precisely adjusted between 0.017 and 0.053 nA. A 30 keV Bi_5^+ beam, operated with a raster of 200 × 200 μm^2 and centered in the sputtered area, was used to record high mass resolution profiles. Its current intensity was precisely adjusted between 0.083 and 0.096 pA. On thick or insulated samples, charging of the surface occurred upon sputtering. When necessary, an electron flood gun was used for charge compensation during the depth profiles. It was operated at 5 or 20 eV.

Design and 3D Printing of Additional Transfer Sample Holders. Several sample holders were printed in polylactic acid (PLA). The design was made with Solidworks, and a Makerbot 2× Replicator (MakerBot Industries, Brooklyn, USA) was used for printing. The different models of transfer sample holders as well as their advantages and disadvantages are listed in the Supporting Information (SI, Table 1). Small 3D print sample holders in PLA do not require additional pumping time in the ToF-SIMS instrument, are stable under vacuum, and allow us to quickly adapt to any type of substrate and geometry.

ASSOCIATED CONTENT

Supporting Information

The Supporting Information is available free of charge at https://pubs.acs.org/doi/10.1021/acsabm.2c00169.

> SIMS chemical images of collectors covered with various proteins; SIMS spectra; size distributions of the cluster beams used for this work; ellipsometry measurements; experimental procedure for the determination of the protein films thickness using the ToF-SIMS instrument; 3D representations of the different sample holder tested, along with their pros and cons; protein deposition rate comparison at 15 and 45°; and additional data regarding the deposition on paper and the construction of multilayers (PDF)

AUTHOR INFORMATION

Corresponding Authors

Christine Dupont-Gillain − *Institute of Condensed Matter and Nanosciences - Bio & Soft Matter, Université catholique de Louvain, B-1348 Louvain-la-Neuve, Belgium;* orcid.org/0000-0002-6153-4044; Email: christine.dupont@uclouvain.be

Arnaud Delcorte − *Institute of Condensed Matter and Nanosciences - Bio & Soft Matter, Université catholique de Louvain, B-1348 Louvain-la-Neuve, Belgium;* orcid.org/0000-0003-4127-8650; Email: arnaud.delcorte@uclouvain.be

Authors

Vincent Delmez − *Institute of Condensed Matter and Nanosciences - Bio & Soft Matter, Université catholique de Louvain, B-1348 Louvain-la-Neuve, Belgium;* orcid.org/0000-0002-9203-9919

https://doi.org/10.1021/acsabm.2c00169
ACS Appl. Bio Mater. 2022, 5, 3180−3192

Benjamin Tomasetti − *Institute of Condensed Matter and Nanosciences - Bio & Soft Matter, Université catholique de Louvain, B-1348 Louvain-la-Neuve, Belgium*
Thomas Daphnis − *Institute of Condensed Matter and Nanosciences - Bio & Soft Matter, Université catholique de Louvain, B-1348 Louvain-la-Neuve, Belgium*
Claude Poleunis − *Institute of Condensed Matter and Nanosciences - Bio & Soft Matter, Université catholique de Louvain, B-1348 Louvain-la-Neuve, Belgium*
Clément Lauzin − *Institute of Condensed Matter and Nanosciences - Bio & Soft Matter, Université catholique de Louvain, B-1348 Louvain-la-Neuve, Belgium*; orcid.org/0000-0001-5044-5137

Complete contact information is available at: https://pubs.acs.org/10.1021/acsabm.2c00169

Author Contributions

[$]V.D. and B.T. contributed equally to this work.

Notes

The authors declare no competing financial interest.

■ ACKNOWLEDGMENTS

The authors acknowledge the financial support by the Fédération Wallonie Bruxelles, through the project "iBEAM" funded by its research program "Actions de Recherche Concertées" (convention no. 18/23-090) and by the Belgian National Foundation for Scientific Research (FNRS) through the Research Foundation for Industry and Agriculture (FRIA). B.T. is a research fellow (ASP) of the FNRS. A.D. is a Research Director of the FNRS.

■ REFERENCES

(1) Sittig, C.; Textor, M.; Spencer, N. D.; Wieland, M.; Vallotton, P. H. Surface Characterization. *J. Mater. Sci.: Mater. Med.* **1999**, *10*, 35−46.
(2) Allara, D. L. A Perspective on Surfaces and Interfaces. *Nature* **2005**, *437*, 638−639.
(3) Kango, S.; Kalia, S.; Celli, A.; Njuguna, J.; Habibi, Y.; Kumar, R. Surface Modification of Inorganic Nanoparticles for Development of Organic−Inorganic Nanocomposites—A Review. *Prog. Polym. Sci.* **2013**, *38*, 1232−1261.
(4) Ratner, B. D.; Castner, D. G. Surface Properties and Surface Characterization of Biomaterials. *Biomater. Sci.* **2020**, 53−75.
(5) Mozetič, M. Surface Modification to Improve Properties of Materials. *Materials* **2019**, *12*, 441.
(6) Ratner, B. D.; Hoffman, A. S.; McArthur, S. L. Physicochemical Surface Modification of Materials Used in Medicine. *Biomater. Sci.* **2020**, 487−505.
(7) Bose, S.; Robertson, S. F.; Bandyopadhyay, A. Surface Modification of Biomaterials and Biomedical Devices Using Additive Manufacturing. *Acta Biomater.* **2018**, *66*, 6−22.
(8) Cho, Y.; Lee, M.; Park, S.; Kim, Y.; Lee, E.; Im, S. G. A Versatile Surface Modification Method via Vapor-Phase Deposited Functional Polymer Films for Biomedical Device Applications. *Biotechnol. Bioprocess Eng.* **2021**, *26*, 165−178.
(9) Leong, H. J.; Oh, S. G. Preparation of Antibacterial TiO2 Particles by Hybridization with Azelaic Acid for Applications in Cosmetics. *J. Ind. Eng. Chem.* **2018**, *66*, 242−247.
(10) Tian, F.; Decker, E. A.; Goddard, J. M. Controlling Lipid Oxidation of Food by Active Packaging Technologies. *Food Funct.* **2013**, *4*, 669−680.
(11) Makvandi, P.; Iftekhar, S.; Pizzetti, F.; Zarepour, A.; Zare, E. N.; Ashrafizadeh, M.; Agarwal, T.; Padil, V. V. T.; Mohammadinejad, R.; Sillanpaa, M.; Maiti, T. K.; Perale, G.; Zarrabi, A.; Rossi, F. Functionalization of Polymers and Nanomaterials for Water Treatment, Food Packaging, Textile and Biomedical Applications: A Review. *Environ. Chem. Lett.* **2020**, *19*, 583−611.
(12) Kian, L. K.; Jawaid, M. Surface Functionalization of Cellulose Biocomposite for Food Packaging Application. *Biopolym. Biocomposites from Agro-Waste Packag. Appl.* **2021**, 255−269.
(13) de Vasconcellos, A.; Miller, A. H.; Aranda, D. A. G.; Nery, J. G. Biocatalysts Based on Nanozeolite-Enzyme Complexes: Effects of Alkoxysilane Surface Functionalization and Biofuel Production Using Microalgae Lipids Feedstock. *Colloids Surf., B* **2018**, *165*, 150−157.
(14) Mitchell, D. T.; Lee, S. B.; Trofin, L.; Li, N.; Nevanen, T. K.; Söderlund, H.; Martin, C. R. Smart Nanotubes for Bioseparations and Biocatalysis. *J. Am. Chem. Soc.* **2002**, *124*, 11864−11865.
(15) Mitchell, S.; Pérez-Ramírez, J. Mesoporous Zeolites as Enzyme Carriers: Synthesis, Characterization, and Application in Biocatalysis. *Catal. Today* **2011**, *168*, 28−37.
(16) Yakimova, R.; Petoral, R. M.; Yazdi, G. R.; Vahlberg, C.; Spetz, A. L.; Uvdal, K. Surface Functionalization and Biomedical Applications Based on SiC. *J. Phys. D: Appl. Phys.* **2007**, *40*, 6435.
(17) Bilek, M. M. M.; Bax, D. V.; Kondyurin, A.; Yin, Y.; Nosworthy, N. J.; Fisher, K.; Waterhouse, A.; Weiss, A. S.; dos Remedios, C. G.; McKenzie, D. R. Free Radical Functionalization of Surfaces to Prevent Adverse Responses to Biomedical Devices. *Proc. Natl. Acad. Sci. U. S. A.* **2011**, *108*, 14405−14410.
(18) Gharibi, R.; Agarwal, S. Favorable Antibacterial, Antibiofilm, Antiadhesion to Cells, and Biocompatible Polyurethane by Facile Surface Functionalization. *ACS Appl. Bio Mater.* **2021**, *4*, 4629−4640.
(19) Oliverio, M.; Perotto, S.; Messina, G. C.; Lovato, L.; De Angelis, F. Chemical Functionalization of Plasmonic Surface Biosensors: A Tutorial Review on Issues, Strategies, and Costs. *ACS Appl. Mater. Interfaces* **2017**, *9*, 29394−29411.
(20) Norde, W. Adsorption of Proteins from Solution at the Solid-Liquid Interface. *Adv. Colloid Interface Sci.* **1986**, *25*, 267−340.
(21) Li, H.; Fierens, K.; Zhang, Z.; Vanparijs, N.; Schuijs, M. J.; Van teendam, K.; Gracia, N. F.; De Rycke, R.; De Beer, T.; De Beuckelaer, A.; De Koker, S.; Deforce, D.; Albertazzi, L.; Grooten, J.; Lambrecht, B. N.; De Geest, B. G. Spontaneous Protein Adsorption on Graphene Oxide Nanosheets Allowing Efficient Intracellular Vaccine Protein Delivery. *ACS Appl. Mater. Interfaces* **2016**, *8*, 1147−1155.
(22) Kang, Y.; Liu, Y. C.; Wang, Q.; Shen, J. W.; Wu, T.; Guan, W. J. On the Spontaneous Encapsulation of Proteins in Carbon Nanotubes. *Biomaterials* **2009**, *30*, 2807−2815.
(23) vander Straeten, A.; Lefèvre, D.; Demoustier-Champagne, S.; Dupont-Gillain, C. Protein-Based Polyelectrolyte Multilayers. *Adv. Colloid Interface Sci.* **2020**, *280*, No. 102161.
(24) Gao, Y.; Kyratzis, I. Covalent Immobilization of Proteins on Carbon Nanotubes Using the Cross-Linker 1-Ethyl-3-(3-Dimethylaminopropyl)Carbodiimide—a Critical Assessment. *Bioconjugate Chem.* **2008**, *19*, 1945−1950.
(25) Williams, R. A.; Blanch, H. W. Covalent Immobilization of Protein Monolayers for Biosensor Applications. *Biosens. Bioelectron.* **1994**, *9*, 159−167.
(26) Bednar, R. M.; Golbek, T. W.; Kean, K. M.; Brown, W. J.; Jana, S.; Baio, J. E.; Karplus, P. A.; Mehl, R. A. Immobilization of Proteins with Controlled Load and Orientation. *ACS Appl. Mater. Interfaces* **2019**, *11*, 36391−36398.
(27) Svalova, T. S.; Medvedeva, M. V.; Kozitsina, A. N. A "Clickable" Electrodeposited Polymer Films Based on 3-Ethynylthiophene for the Covalent Immobilization of Proteins. Application to a Label-Free Electrochemical Immunosensor for Escherichia Coli and Staphylococcus Aureus Determination. *Electroanalysis* **2021**, *33*, 2469−2475.
(28) Schneider, A.-K.; Nikolov, P. M.; Giselbrecht, S.; Niemeyer, C. M.; Schneider, A.; Nikolov, P. M.; Niemeyer, C. M.; Giselbrecht, S. DNA-SMART: Biopatterned Polymer Film Microchannels for Selective Immobilization of Proteins and Cells. *Small* **2017**, *13*, 1603923.
(29) Li, M.; Yue, Y.; Zhang, Z. J.; Wang, Z. Y.; Tan, T. W.; Fan, L. H. Site-Specific and High-Loading Immobilization of Proteins by

Using Cohesin-Dockerin and CBM-Cellulose Interactions. *Bioconjugate Chem.* **2016**, *27*, 1579−1583.
(30) Zare-Eelanjegh, E.; Bora, D. K.; Rupper, P.; Schrantz, K.; Thöny-Meyer, L.; Maniura-Weber, K.; Richter, M.; Faccio, G. Affinity-Driven Immobilization of Proteins to Hematite Nanoparticles. *ACS Appl. Mater. Interfaces* **2016**, *8*, 20432−20439.
(31) Liu, Y.; Tao, F.; Miao, S.; Yang, P. Controlling the Structure and Function of Protein Thin Films through Amyloid-like Aggregation. *Acc. Chem. Res.* **2021**, *54*, 3016−3027.
(32) Wang, D.; Ha, Y.; Gu, J.; Li, Q.; Zhang, L.; Yang, P.; Wang, D.; Ha, Y.; Gu, J.; Li, Q.; Yang, P.; Zhang, L. 2D Protein Supramolecular Nanofilm with Exceptionally Large Area and Emergent Functions. *Adv. Mater.* **2016**, *28*, 7414−7423.
(33) Xu, Y.; Liu, Y.; Hu, X.; Qin, R.; Su, H.; Li, J.; Yang, P. The Synthesis of a 2D Ultra-Large Protein Supramolecular Nanofilm by Chemoselective Thiol−Disulfide Exchange and Its Emergent Functions. *Angew. Chem., Int. Ed.* **2020**, *59*, 2850−2859.
(34) Lundqvist, M.; Sethson, I.; Jonsson, B.-H. Protein Adsorption onto Silica Nanoparticles: Conformational Changes Depend on the Particles' Curvature and the Protein Stability. *Langmuir* **2004**, *20*, 10639−10647.
(35) Norde, W. My Voyage of Discovery to Proteins in Flatland ...and Beyond. *Colloids Surf., B* **2008**, *61*, 1−9.
(36) Norde, W.; Horbett, T. A., Brash, J. L. Proteins at Interfaces III: Introductory Overview. In *Proteins at Interfaces III State of the Art*; ACS Publications, 2012; pp. 1−34.
(37) Denis, F. A.; Hanarp, P.; Sutherland, D. S.; Gold, J.; Mustin, C.; Rouxhet, P. G.; Dufrêne, Y. F. Protein Adsorption on Model Surfaces with Controlled Nanotopography and Chemistry. *Langmuir* **2002**, *18*, 819−828.
(38) Denis, F. A.; Pallandre, A.; Nysten, B.; Jonas, A. M.; Dupont-Gillain, C. C. Alignment and Assembly of Adsorbed Collagen Molecules Induced by Anisotropic Chemical Nanopatterns. *Small* **2005**, *1*, 984−991.
(39) Falconnet, D.; Csucs, G.; Grandin, H. M.; Textor, M. Surface Engineering Approaches to Micropattern Surfaces for Cell-Based Assays. *Biomaterials* **2006**, *27*, 3044−3063.
(40) Franchetti, V.; Solka, B. H.; Baitinger, W. E.; Amy, J. W.; Cooks, R. G. Soft Landing of Ions as a Means of Surface Modification. *Int. J. Mass Spectrom. Ion Phys.* **1977**, *23*, 29−35.
(41) Tata, A.; Salvitti, C.; Pepi, F. From Vacuum to Atmospheric Pressure: A Review of Ambient Ion Soft Landing. *Int. J. Mass Spectrom.* **2020**, *450*, 116309.
(42) Su, P.; Hu, H.; Warneke, J.; Belov, M. E.; Anderson, G. A.; Laskin, J. Design and Performance of a Dual-Polarity Instrument for Ion Soft Landing. *Anal. Chem.* **2019**, *91*, 5904−5912.
(43) Grill, V.; Shen, J.; Evans, C.; Cooks, R. G. Collisions of Ions with Surfaces at Chemically Relevant Energies: Instrumentation and Phenomena. *Rev. Sci. Instrum.* **2001**, *72*, 3149.
(44) Johnson, G. E.; Gunaratne, D.; Laskin, J. Soft-and Reactive Landing of Ions onto Surfaces: Concepts and Applications. *Mass Spectrom. Rev.* **2016**, *35*, 439−479.
(45) Laskin, J.; Johnson, G. E.; Warneke, J.; Prabhakaran, V. From Isolated Ions to Multilayer Functional Materials Using Ion Soft Landing. *Angew. Chem., Int. Ed.* **2018**, *57*, 16270−16284.
(46) Rauschenbach, S.; Ternes, M.; Harnau, L.; Kern, K. Mass Spectrometry as a Preparative Tool for the Surface Science of Large Molecules. *Annu. Rev. Anal. Chem.* **2016**, *9*, 473−498.
(47) Verbeck, G.; Hoffmann, W.; Walton, B. Soft-Landing Preparative Mass Spectrometry. *Analyst* **2012**, *137*, 4393−4407.
(48) Deng, Z.; Thontasen, N.; Malinowski, N.; Rinke, G.; Harnau, L.; Rauschenbach, S.; Kern, K. A Close Look at Proteins: Submolecular Resolution of Two- and Three-Dimensionally Folded Cytochrome c at Surfaces. *Nano Lett.* **2012**, *12*, 2452−2458.
(49) Ouyang, Z.; Takáts, Z.; Blake, T. A.; Gologan, B.; Guymon, A. J.; Wiseman, J. M.; Oliver, J. C.; Davisson, V. J.; Cooks, R. G. Preparing Protein Microarrays by Soft-Landing of Mass-Selected Ions. *Science* **2003**, *301*, 1351−1354.
(50) Gologan, B.; Takáts, Z.; Alvarez, J.; Wiseman, J. M.; Talaty, N.; Ouyang, Z.; Cooks, R. G. Ion Soft-Landing into Liquids: Protein Identification, Separation, and Purification with Retention of Biological Activity. *J. Am. Soc. Mass Spectrom.* **2004**, *15*, 1874−1884.
(51) Salvitti, C.; Troiani, A.; Mazzei, F.; D'Agostino, C.; Zumpano, R.; Baldacchini, C.; Bizzarri, A. R.; Tata, A.; Pepi, F. The Use of a Commercial ESI Z-Spray Source for Ambient Ion Soft Landing and Microdroplet Reactivity Experiments. *Int. J. Mass Spectrom.* **2021**, *468*, 116658.
(52) Yamada, I.; Matsuo, J.; Toyoda, N.; Kirkpatrick, A. Materials Processing by Gas Cluster Ion Beams. *Mater. Sci. Eng. R: Rep.* **2001**, *34*, 231−295.
(53) Yamada, I.; Matsuo, J.; Insepov, Z.; Aoki, T.; Seki, T.; Toyoda, N. Nano-Processing with Gas Cluster Ion Beams. *Nucl. Instrum. Methods Phys. Res., Sect. B* **2000**, *164-165*, 944−959.
(54) Yamada, I.; Toyoda, N. Nano-Scale Surface Modification Using Gas Cluster Ion Beams — A Development History and Review of the Japanese Nano-Technology Program. *Surf. Coat. Technol.* **2007**, *201*, 8579−8587.
(55) Toyoda, N.; Yamada, I. Gas Cluster Ion Beam Equipment and Applications for Surface Processing. *IEEE Trans. Plasma Sci.* **2008**, *36*, 1471−1488.
(56) Toyoda, N.; Hagiwara, N.; Matsuo, J.; Yamada, I. Surface Smoothing Mechanism of Gas Cluster Ion Beams. *Nucl. Instrum. Methods Phys. Res., Sect. B* **2000**, *161-163*, 980−985.
(57) Winograd, N. The Magic of Cluster SIMS. *Anal. Chem.* **2005**, *77*, 142 A−149 A.
(58) Rabbani, S.; Barber, A. M.; Fletcher, J. S.; Lockyer, N. P.; Vickerman, J. C. TOF-SIMS with Argon Gas Cluster Ion Beams: A Comparison with C 60. *Anal. Chem.* **2011**, *83*, 3793−3800.
(59) Delcorte, A.; Cristaudo, V.; Lebec, V.; Czerwinski, B. Sputtering of Polymers by KeV Clusters: Microscopic Views of the Molecular Dynamics. *Int. J. Mass Spectrom.* **2014**, *370*, 29−38.
(60) Delcorte, A.; Debongnie, M. Macromolecular Sample Sputtering by Large Ar and CH4 Clusters: Elucidating Chain Size and Projectile Effects with Molecular Dynamics. *J. Phys. Chem. C* **2015**, *119*, 25868−25879.
(61) Delcorte, A.; Delmez, V.; Dupont-Gillain, C.; Lauzin, C.; Jefford, H.; Chundak, M.; Poleunis, C.; Moshkunov, K. Large Cluster Ions: Soft Local Probes and Tools for Organic and Bio Surfaces. *Phys. Chem. Chem. Phys.* **2020**, *22*, 17427−17447.
(62) Ninomiya, S.; Nakata, Y.; Ichiki, K.; Seki, T.; Aoki, T.; Matsuo, J. Measurements of Secondary Ions Emitted from Organic Compounds Bombarded with Large Gas Cluster Ions. *Nucl. Instrum. Methods Phys. Res., Sect. B* **2007**, *256*, 493−496.
(63) Oshima, S.; Kashihara, I.; Moritani, K.; Inui, N.; Mochiji, K. Soft-Sputtering of Insulin Films in Argon-Cluster Secondary Ion Mass Spectrometry. *Rapid Commun. Mass Spectrom.* **2011**, *25*, 1070−1074.
(64) Mochiji, K.; Hashinokuchi, M.; Moritani, K.; Toyoda, N. Matrix-Free Detection of Intact Ions from Proteins in Argon-Cluster Secondary Ion Mass Spectrometry. *Rapid Commun. Mass Spectrom.* **2009**, *23*, 648−652.
(65) Lorenz, M.; Shard, A. G.; Counsell, J. D. P.; Hutton, S.; Gilmore, I. S. Angular Distribution of Molecules Sputtered by Gas Cluster Ion Beams and Implications for Secondary Neutral Mass Spectrometry. *J. Phys. Chem. C* **2016**, *120*, 25317−25327.
(66) Lorenz, M.; Zhang, J.; Shard, A. G.; Vorng, J. L.; Rakowska, P. D.; Gilmore, I. S. Method for Molecular Layer Deposition Using Gas Cluster Ion Beam Sputtering with Example Application in Situ Matrix-Enhanced Secondary Ion Mass Spectrometry. *Anal. Chem.* **2021**, *93*, 3436−3444.
(67) Moshkunov, K.; Tomasetti, B.; Daphnis, T.; Delmez, V.; Vanvarenberg, K.; Préat, V.; Lorenz, M.; Quanico, J.; Baggerman, G.; Lemiere, F.; Dupont, C.; Delcorte, A. Improvement of Biomolecular Analysis in Thin Films Using in Situ Matrix Enhanced Secondary Ion Mass Spectrometry. *Analyst* **2021**, *146*, 6506−6519.
(68) Delmez, V.; Degand, H.; Poleunis, C.; Moshkunov, K.; Chundak, M.; Dupont-Gillain, C.; Delcorte, A. Deposition of Intact

https://doi.org/10.1021/acsabm.2c00169
ACS Appl. Bio Mater. 2022, 5, 3180−3192

and Active Proteins In Vacuo Using Large Argon Cluster Ion Beams. *J. Phys. Chem. Lett.* **2021**, *12*, 952−957.
(69) Weibel, D. E.; Lockyer, N.; Vickerman, J. C. C60 Cluster Ion Bombardment of Organic Surfaces. *Appl. Surf. Sci.* **2004**, *231*−*232*, 146−152.
(70) Seah, M. P.; Spencer, S. J.; Shard, A. G. Angle Dependence of Argon Gas Cluster Sputtering Yields for Organic Materials. *J. Phys. Chem. B* **2015**, *119*, 3297−3303.
(71) Cristaudo, V.; Poleunis, C.; Laha, P.; Eloy, P.; Hauffman, T.; Terryn, H.; Delcorte, A. Applied Surface Science Ion Yield Enhancement at the Organic / Inorganic Interface in SIMS Analysis Using Ar-GCIB. *Appl. Surf. Sci.* **2021**, *536*, 147716.
(72) Delcorte, A.; Bertrand, P.; Arys, X.; Jonas, A.; Wischerhoff, E.; Mayer, B.; Laschewsky, A. ToF-SIMS Study of Alternate Polyelectrolyte Thin Films: Chemical Surface Characterization and Molecular Secondary Ions Sampling Depth. *Surf. Sci.* **1996**, *366*, 149−165.
(73) Szakal, C.; Kozole, J.; Russo, M. F.; Garrison, B. J.; Winograd, N. Surface Sensitivity in Cluster-Ion-Induced Sputtering. *Phys. Rev. Lett.* **2006**, *96*, 216104.
(74) Delcorte, A. A Microscopic View of Macromolecule Transfer in the Vacuum Using Gas and Bismuth Clusters. *J. Phys. Chem. C* **2022**, *126*, 7307−7318.

https://doi.org/10.1021/acsabm.2c00169
ACS Appl. Bio Mater. 2022, 5, 3180−3192